

Journal of Visualized Experiments

Microfluidic Platform with Multiplexed Electronic Detection for Spatial Tracking of Particles --Manuscript Draft--

Manuscript Number:	JoVE55311R1
Full Title:	Microfluidic Platform with Multiplexed Electronic Detection for Spatial Tracking of Particles
Article Type:	Invited Methods Article - JoVE Produced Video
Keywords:	lab-on-a-chip; microfluidics; multiplexed cytometry; spatial cell tracking; resistive pulse sensing; Coulter counter; CDMA; orthogonal detection.
Manuscript Classifications:	10.1.897.520.500.500: Microfluidics; 5.5.196.630.465: Microfluidic Analytical Techniques; 5.5.588.465: Microfluidic Analytical Techniques
Corresponding Author:	Ali Fatih Sarioglu Georgia Institute of Technology Atlanta, GA UNITED STATES
Corresponding Author Secondary Information:	
Corresponding Author E-Mail:	sarioglu@gatech.edu
Corresponding Author's Institution:	Georgia Institute of Technology
Corresponding Author's Secondary Institution:	
First Author:	Ningquan Wang
First Author Secondary Information:	
Other Authors:	Ningquan Wang Ruxiu Liu
Order of Authors Secondary Information:	
Abstract:	Microfluidic processing of biological samples typically involves differential manipulations of suspended particles under various force fields in order to spatially fractionate the sample based on a biological property of interest. For the resultant spatial distribution to be used as the assay readout, microfluidic devices are often subjected to microscopic analysis requiring complex instrumentation with higher cost and reduced portability. To address this limitation, we have developed an integrated electronic sensing technology for multiplexed detection of particles at different locations on a microfluidic chip. Our technology, called Microfluidic CODES, combines Resistive Pulse Sensing with Code Division Multiple Access to compress 2D spatial information into a 1D electrical signal. In this paper, we present a practical demonstration of the Microfluidic CODES technology to detect and size cultured cancer cells distributed over multiple microfluidic channels. As validated by the high-speed microscopy, our technology can accurately analyze dense cell populations all electronically without the need for an external instrument. As such, the Microfluidic CODES can potentially enable low-cost integrated lab-on-a-chip devices that are well suited for the point-of-care testing of biological samples.
Author Comments:	
Additional Information:	
Question	Response
If this article needs to be "in-press" by a certain date, please indicate the date below and explain in your cover letter.	

TITLE:

Microfluidic Platform with Multiplexed Electronic Detection for Spatial Tracking of Particles

AUTHORS:

Wang, Ningquan

School of Electrical and Computer Engineering

Georgia Institute of Technology

Atlanta, GA, USA

nwang79@gatech.edu

Liu, Ruxiu

School of Electrical and Computer Engineering

Georgia Institute of Technology

Atlanta, GA, USA

rliu76@gatech.edu

Sarioglu, A. Fatih

School of Electrical and Computer Engineering

Institute of Electronics and Nanotechnology

Petit Institute for Bioengineering and Biosciences

Georgia Institute of Technology

Atlanta, GA, USA

sarioglu@gatech.edu

CORRESPONDING AUTHOR:

Sarioglu, A. Fatih

sarioglu@gatech.edu

KEYWORDS:

lab-on-a-chip, microfluidics, multiplexed cytometry, spatial cell tracking, resistive pulse sensing, Coulter counter, CDMA, orthogonal detection

SHORT ABSTRACT:

We demonstrate a microfluidic platform with an integrated surface electrode network that combines resistive pulse sensing (RPS) with code division multiple access (CDMA), to multiplex detection and sizing of particles in multiple microfluidic channels.

LONG ABSTRACT:

Microfluidic processing of biological samples typically involves differential manipulations of suspended particles under various force fields in order to spatially fractionate the sample based on a biological property of interest. For the resultant spatial distribution to be used as the assay readout, microfluidic devices are often subjected to microscopic analysis requiring complex instrumentation with higher cost and reduced portability. To address this limitation, we have developed an integrated electronic sensing technology for multiplexed detection of particles at

different locations on a microfluidic chip. Our technology, called Microfluidic CODES, combines Resistive Pulse Sensing with Code Division Multiple Access to compress 2D spatial information into a 1D electrical signal. In this paper, we present a practical demonstration of the Microfluidic CODES technology to detect and size cultured cancer cells distributed over multiple microfluidic channels. As validated by the high-speed microscopy, our technology can accurately analyze dense cell populations all electronically without the need for an external instrument. As such, the Microfluidic CODES can potentially enable low-cost integrated lab-on-a-chip devices that are well suited for the point-of-care testing of biological samples.

INTRODUCTION:

Accurate detection and analysis of biological particles such as cells, bacteria or viruses suspended in liquid is of great interest for a range of applications¹⁻³. Well-matched in size, microfluidic devices offer unique advantages for this purpose such as high-sensitivity, gentle sample manipulation and well-controlled microenvironment⁴⁻⁷. In addition, microfluidic devices can be designed to employ a combination of fluid dynamics and force fields to passively fractionate a heterogeneous population of biological particles based on various properties⁸⁻¹². In those devices, the resultant particle distribution can be used as readout but spatial information is typically accessible only through microscopy, limiting the practical utility of the microfluidic device by tying it to a lab infrastructure. Therefore, an integrated sensor that can readily report particles' spatiotemporal mapping, as they are manipulated on a microfluidic device, can potentially enable low-cost, integrated lab-on-a-chip devices that are particularly attractive for the testing of samples in mobile, resource-limited settings.

Thin film electrodes have been used as integrated sensors in microfluidic devices for various applications¹³⁻¹⁴. Resistive Pulse Sensing (RPS) is particularly attractive for integrated sensing of small particles in microfluidic channels as it offers a robust, sensitive, and high-throughput detection mechanism directly from electrical measurements¹⁵. In RPS, the impedance modulation between a pair of electrodes, immersed in an electrolyte, is used as a means to detect a particle. When the particle passes through an aperture, sized on the order of the particle, the number and amplitude of transient pulses in the conduction are used to count and size particles, respectively. Moreover, the sensor geometry can be designed with a photolithographic resolution to shape resistive pulse waveforms in order to enhance sensitivity¹⁶⁻¹⁹ or to estimate vertical position of particles in microfluidic channels²⁰.

We have recently introduced a scalable and simple multiplexed resistive pulse sensing technology called Microfluidic Coded Orthogonal Detection by Electrical Sensing (Microfluidic CODES)²¹. Microfluidic CODES relies on an interconnected network of resistive pulse sensors, each consisting of an array of electrodes micromachined to modulate conduction in a unique, distinguishable manner, so as to enable multiplexing. We have specifically designed each sensor to produce orthogonal electrical signals similar to the digital codes used in code division multiple access²² (CDMA) telecommunication networks, so that individual resistive pulse sensor signal can be uniquely recovered from a single output waveform, even if signals from different sensors interfere. In this way, our technology compresses 2D spatial information of particles

into a 1D electrical signal, permitting monitoring of particles at different locations on a microfluidic chip, while keeping both device- and system-level complexity to a minimum.

In this paper, we present a detailed protocol for experimental and computational methods necessary to use the Microfluidic CODES technology, as well as representative results from its use in analysis of simulated biological samples. Using the results from a prototype device with four multiplexed sensors as an example to explain the technique, we provide protocols on (1) the microfabrication process to create microfluidic devices with the Microfluidic CODES technology (2) the description of the experimental setup including the electronic, optical, and fluidic hardware (3) the computer algorithm for decoding interfering signals from different sensors, and (4) the results from detection and analysis of cancer cells in microfluidic channels. We believe that using the detailed protocol described here, other researchers can apply our technology for their research.

PROTOCOL:

1. Design of coding electrodes

Note: Figure 1a shows the 3-D structure of the micropatterned electrodes.

1.1) Design a set of four 7-bit Gold codes for encoding the microfluidic channels²³.

1.1.1) Construct two linear feedback shift-registers (LFSRs), each representing a primitive polynomial.

1.1.2) Use the LFSRs to generate a preferred pair of 7-bit m -sequences.

1.1.3) Cyclically shift the preferred pair of m -sequences and add them in mod 2 to generate four distinct Gold codes.

1.2) Design the layout of the coding electrodes (**Figure 1b**).

1.2.1) Place three electrode terminals, representing the positive, negative, and reference electrodes at three corners.

1.2.2) Route positive and negative electrode traces on opposite sides of each microfluidic channel.

1.2.3) Extend positive and negative electrodes into the microfluidic channels as electrode fingers, following the uniquely assigned Gold code (**Figure 1c**).

1.2.4) Place the reference electrode in between the positive and negative electrode fingers.

1.2.5) Place positive and negative electrode traces far from the outermost reference electrode fingers in order to minimize electrical conduction outside the coding region.

2. Microfabrication of surface electrodes

Note: Figure 2b shows the fabrication process of surface electrodes.

2.1) Clean a 4-inch borosilicate glass wafer in a piranha solution (98% sulfuric acid: 30% hydrogen peroxide = 5:1) at 120 °C for 20 min to remove all the organic contaminants. Then place the wafer on a 200 °C hot plate for 20 min to remove residual water.

2.2) Transfer the wafer to a spinner. Dispense 2 mL negative photoresist onto the wafer and spin the wafer at a speed of 3000 rpm for 40 s to uniformly coat the wafer with a 1.5- μm photoresist layer.

2.3) Place the wafer on a 150 °C hot plate and bake the spun photoresist for 1 min.

2.4) Expose the photoresist to 365-nm UV light (225 mJ/cm²) through a chrome mask using a mask aligner.

2.5) Place the wafer on a 100 °C hot plate and bake the exposed photoresist for 1 min.

2.6) Develop the photoresist by immersing the wafer in a photoresist developer (RD6) for 15 s. Gently spray deionized (DI) water and wash the wafer. Dry by blowing compressed nitrogen.

2.7) Place the wafer with patterned photoresist into an e-beam metal evaporator, and deposit a 20-nm-thick chrome film, followed by an 80-nm-thick gold film onto the wafer at a base pressure of 3×10^{-6} Torr with a deposition rate of 1 Å/s.

2.8) Immerse the metal-coated wafer into acetone in an ultrasonic bath set at a frequency of 40 kHz with 100% amplitude for 30 min at room temperature to etch the underlying photoresist and complete the lift-off process.

2.9) Dice the wafer into smaller pieces using a conventional dicing saw.

3. Fabrication of the SU-8 mold for microfluidic channels

Note: Figure 2a shows the fabrication process of the mold for microfluidic channels.

3.1) Clean and bake a 4-inch silicon wafer using the same procedure described in 2.1.

3.2) Coat the wafer with photoresist. Transfer the wafer to a spinner. Pour 4 mL photoresist onto the wafer.

3.2.1) Spin the wafer at 500 rpm for 15 s.

3.2.2) Spin the wafer at 1000 rpm for 15 s.

3.2.3) Spin the wafer at 3000 rpm for 60 s to obtain a uniformly coated 15- μm thick photoresist layer.

3.3) Place the wafer face up on a cleanroom wipe soaked in acetone and remove the residual photoresist from the backside and edges of the wafer.

3.4) Transfer the wafer onto a hot plate for soft baking. First, bake the wafer at 65 °C for 1 min. Then quickly move the wafer to a 95 °C hot plate and bake for 2 min.

3.5) Expose the photoresist to 365-nm UV light (180 mJ/cm²) through a chrome mask by using a mask aligner.

3.6) Bake the wafer following exposure at 65 °C for 1 min and then at 95 °C for 2 min.

3.7) Immerse the wafer in developer and gently shake the container for 3 min. Then, rinse the wafer with isopropanol alcohol (IPA) and dry it by blowing compressed nitrogen. If a white-colored residue appears on the wafer, immerse it into the developer again and develop for longer time and dry.

3.8) Bake the wafer on a 200 °C hot plate for 30 min to dry it completely.

3.9) Measure the thickness of the patterned photoresist using a profilometer at different locations across the wafer to ensure uniformity.

3.10) Silanize the mold wafer by utilizing the technique of vapor deposition. Add 200 μL of trichlorosilane in a petri dish and place in a vacuum desiccator along with the SU-8 mold wafer for 8 hours.

4. Assembly of the Microfluidic CODES device

4.1) Place the 4-inch silicon wafer with the mold in a 150-mm diameter petri dish, and fix it by taping from its edges.

4.2) Mix the polydimethylsiloxane (PDMS) pre-polymer and cross-linker at a ratio of 10:1, and pour 50 g of the mixture into the petri dish. Place the petri dish in a vacuum desiccator to degas the mixture for 1 hour, and then cure it in an oven at 65 °C for at least 4 hours (**Figure 2a**).

4.3) Cut out the cured PDMS layer using a scalpel and peel it off the mold wafer using a tweezer. The size of the proof-of-principle device is approximately 20 mm \times 7 mm. Then punch holes with a diameter of 1.5 mm through the PDMS for the inlet and outlet of the microfluidic channel using a biopsy puncher.

4.4) Clean the patterned side of the PDMS part by placing it on a clean-room adhesive tape.

4.5) Clean the glass substrate with surface electrodes by rinsing it with acetone, IPA, DI water and dry using compressed nitrogen.

4.6) Activate the surfaces of PDMS and glass substrate in oxygen plasma for 30 s with the micromachined side of each part facing up in an RF plasma generator set at 100 mW.

4.7) Align the PDMS microfluidic channel with surface electrodes on the glass substrate using an optical microscope and then bring the two plasma-activated surfaces in physical contact.

4.8) Bake the device on a 70 °C hot plate for 5 min, with the glass side facing the hot plate.

4.9) Connect the contact pads of the electrodes with wires by soldering.

5. Preparation of the simulated biological sample

5.1) Culture the HeyA8 human ovarian cancer cells in RPMI 1640 supplemented with 10% FBS and 1% penicillin-streptomycin in 5% CO₂ atmosphere at 37 °C until they reach 80% confluence.

5.2) Aspirate the media from the culture flask using a glass pipette. Dispense and then aspirate 1X phosphate buffered saline (PBS) to wash the cells.

5.3) Incubate cells in 2 mL 0.05% (w/v) trypsin solution for 2 min at 37 °C to suspend adherent cells. Then, add 4 mL of the culture media to neutralize the trypsin.

5.4) Centrifuge the cell suspension at 100 x g for 5 min to pellet the cells in a test tube. Then, aspirate supernatant completely.

5.5) Re-suspend the cells in 1-2 mL 1X PBS by gently pipetting up and down to mechanically dissociate cell clumps.

5.6) Draw a small amount of cell suspension into a pipette and count the number of cells using hemocytometer.

5.7) Dilute the cell suspension with PBS to prepare a sample with final cell concentration of 10⁵-10⁶ cells/mL.

6. Running the Microfluidic CODES device

Note: Figure 3 shows the experimental setup.

6.1) Place the Microfluidic CODES device on the stage of an optical microscope.

6.2) Apply a 400 kHz sine wave to the reference electrode on the chip using an electronic function generator.

6.3) Connect positive and negative sensing electrodes to two independent trans-impedance amplifiers to convert current signals from each to voltage signals.

6.4) Subtract the positive sensing electrode voltage signal from the negative sensing electrode voltage signal using a differential voltage amplifier in order to obtain a bipolar signal.

6.5) Use a high-speed camera to optically record operation of the device for validation and characterization purposes.

6.6) Drive the cell suspension through the Microfluidic CODES device at a constant flow rate (50-1000 $\mu\text{L/h}$) using a syringe pump.

6.7) Measure the impedance modulation signal using a lock-in amplifier.

6.7.1) Connect the reference AC signal to the reference input of the lock-in amplifier. Connect the differential bipolar signal to the lock-in amplifier as input signal.

6.7.2) Obtain the RMS amplitude of the differential signal from the lock-in amplifier output.

6.8) Sample the lock-in amplifier output signal at 1 MHz rate into a computer through a data acquisition board for further analysis.

7. Processing of sensor signals

7.1) Transfer recorded electrical data into MATLAB for post-processing and decoding.

7.2) Filter the recorded signal in the digital domain using a Butterworth filter (MATLAB built-in function) to remove the high frequency noise (>2.5 kHz).

7.3) Generate a template code library from sensor signals.

7.3.1) Identify representative non-overlapping code signals corresponding to each sensor in the device and extract these signal blocks from the dataset as separate waveform vectors.

7.3.2) Normalize each template code waveform vector by its power. Use the MATLAB built-in function (bandpower) to measure the signal power.

7.3.3) Use MATLAB function (resample) to expand the template library by digitally creating versions of normalized code signals with varying durations to accommodate variations in the cell flow speed over the electrodes.

7.4) Identify the signal blocks that correspond to sensor activity (threshold: $\text{SNR} > 12$ dB) in the filtered waveform. Waveform with SNR under the threshold would be treated as noise.

7.5) Decode individual blocks of sensor activity in the recorded signal by using an iterative

algorithm based on the successive interference cancellation, a technique commonly employed in multi-user CDMA communication networks²⁴⁻²⁵.

7.5.1) Calculate cross-correlation of each signal block with all of the templates in the library using sliding dot product.

7.5.2) Identify the template that produces the largest auto-correlation peak to determine the dominant individual sensor code signal. Record the both time and amplitude of the autocorrelation peak.

7.5.3) Construct an estimate sensor code signal by scaling the identified code template based on the measured autocorrelation peak amplitude and timing information (determined in step 7.5.2).

7.5.4) Subtract the estimated sensor code signal from the original data.

7.5.5) Iterate the process from 7.5.1, until the residual signal does not resemble any signal in the template library, mathematically defined as the correlation coefficient being less than 0.5.

7.6) Refine initial sensor signal estimations from step 7.5 using an optimization process.

7.6.1) Reconstruct the signal by adding estimated individual sensor signals from each iteration.

7.6.2) Sweep the amplitude, duration and timing of individual sensor signals around the original estimates to produce the best fit with the recorded electrical signal based on least-squares approximation²⁶.

7.7) Convert amplitudes of estimated sensor signals into cell size by calibrating electrical signals against optical images.

REPRESENTATIVE RESULTS:

A Microfluidic CODES device consisting of four sensors distributed over four microfluidic channels is shown in **Figure 1b**. In this system, the cross-section of each microfluidic channel was designed to be close to the size of a cell so that (1) multiple cells cannot pass over the electrodes in parallel and (2) cells remain close to the electrodes increasing the sensitivity. Each sensor is designed to generate a unique 7-bit digital code. The device was then tested using a cell suspension. Recorded electrical signals corresponding to four individual sensors are shown with associated ideal digital codes in **Figure 4**. Recorded signals closely match with the ideal square pulses, while small deviations do exist. Such deviations result from a combination of several factors including the non-uniform electric field between coplanar electrodes, coupling between different electrode pairs, spherical shape of cells, as well as the constant flow speed of cells in microfluidic channels. We created a template library based on the recoded sensor signals. By correlating the recorded signals with all of the templates in the library, we determined a template that produced the maximum auto-correlation peak (**Figure 4**). As the

digital codes for microfluidic channels are designed to be orthogonal to each other, a dominant auto-correlation peak could robustly be identified in this process. Using this approach, we could computationally determine the microfluidic channel the cell passed through, the duration of the sensor signal, and therefore the flow speed of the cell.

The Microfluidic CODES technology can resolve situations when multiple cells simultaneously interact with coding electrodes. When such overlaps occur, the signals from individual sensors interfere and the resultant waveform cannot readily be associated with any single template corresponding to a specific sensor. Accurately decoding such overlapping signals is particularly important for reliable processing high-density samples, where interferences are more likely to occur. To resolve overlapping events, we developed an iterative algorithm based on a successive interference cancellation (SIC) scheme²⁴⁻²⁵, which is typically used for multi-user detection in CDMA communication networks. **Figure 5** demonstrates how the SIC algorithm is implemented in resolving a waveform that resulted from four overlapping cells in four different microfluidic channels. In each iteration, we first determined the dominant auto-correlation peak (**Figure 5a**, 2nd column), corresponding to the strongest interfering signal, by correlating the input waveform (**Figure 5a**, 1st column) with the template library. Based on the selected template and the resultant auto-correlation amplitude, we then estimated the strongest interfering signal (**Figure 5a**, 3rd column) and subtracted it from the input waveform. The remaining waveform was passed to the next iteration as the input. This process continued until the correlation of the residual signal with the template library did not produce a clear auto-correlation peak (**Figure 5a**, 5th row, 2nd plot). Following the termination of the interference cancellation process, we reconstructed an estimate of the waveform by combining all the estimated signals from each iteration (**Figure 6a**). Using an optimization process based on a least squares approximation to minimize the mean square error between the original waveform and the reconstructed signal, we updated our estimates for the amplitude, duration, and relative timing of individual sensor code signals (**Figure 6b**). We also estimated the size of the cells detected based on the amplitude of the estimated individual sensor signals. To achieve this, we calibrated the electrical signal amplitudes with optically measured cell sizes using linear regression (**Figure 6b**). A comparison of our results from the Microfluidic CODES with the information obtained from the simultaneously recorded high-speed microscope images shows that the cell size and speed can be accurately measured, which validates our results (**Table 1**). **Figure 6c** shows the simultaneously recorded high-speed microscopy image used for validating the decoding result.

To demonstrate the reproducibility of our results and also the performance of the Microfluidic CODES technology for a high-throughput sample processing, we analyzed electrical signals corresponding to >1000 cells. The signals were automatically decoded in MATLAB by running the algorithm explained above and the accuracy of our results was evaluated by directly comparing our results with optical data from simultaneously recorded high-speed video. Our analysis indicates that electrical signals from 96.15% of cells (973/1012) were accurately decoded. Success rate for decoding non-overlapping and overlapping cell signals is 98.71% (688/697) and 90.48% (285/315), respectively.

Figure 1: Design of the four-channel Microfluidic CODES device.

(a) Electrodes in each microfluidic channel are micropatterned to generate a unique digital code. The impedance modulation due to sequential interactions of flowing cells with electrode pairs leads to electrical pulses. (b) A microscope image of the Microfluidic CODES device. During the fabrication process, glass substrate with coding surface electrodes is aligned with PDMS microfluidic channels under a microscope. (c) A close-up image of coded surface electrodes producing 7-bit Gold sequences: “1010110”, “0111111”, “0100010”, “0011000”

Figure 2: Microfabrication process.

(a) The PDMS microfluidic channels are fabricated using soft lithography²⁷. (b) The surface electrodes are fabricated using a lift-off process. (c) A cross-sectional schematic of the final device. PDMS microfluidic channels are aligned and bonded to the glass substrate with surface electrodes.

Figure 3: Experimental setup.

Using a syringe pump, the cell suspension is run through the Microfluidic CODES device at a constant flow rate. A 400 kHz AC signal is applied to the reference electrode using a function generator. Current signals from positive and negative sensing electrodes are first converted into voltage signals using two transimpedance amplifiers and subtracted from each other using a differential amplifier. The differential bipolar signal is extracted by a lock-in amplifier and then sampled into a computer for signal processing and decoding. High-speed optical microscopy is used to optically record operation of the device for validation and characterization purposes.

Figure 4: Recorded electrical signals from individual sensors and their correlations.

Recorded signals and their correlation with each other are given for four code-multiplexed resistive pulse sensors. Sensor 1 (a), sensor 2 (b), sensor 3 (c) and sensor 4 (d) were designed to produce 7-bit digital waveforms “1010110”, “0111111”, “0100010”, and “0011000”, respectively. For each sensor, the top figure shows that normalized signal recorded from each sensor matches closely with the ideal square pulse sequence that the sensor was designed to produce. For each sensor, the lower panel shows recorded sensor signal’s autocorrelation and cross-correlation with signals corresponding to three other code-multiplexed sensors in the network. In all cases, an autocorrelation peak can robustly be identified because the digital codes from individual sensors are designed to be orthogonal to each other.

Figure 5: Decoding an overlapping waveform with successive interference cancellation.

In each iteration, the input waveform (1st column) is correlated with the preassembled template library to identify the specific template that results in the maximum correlation amplitude (2nd column). Using this specific template, the strongest interfering signal is estimated based on the amplitude and timing information from the correlation peak (3rd column). The estimated signal is then subtracted from the original waveform, effectively canceling the strongest interference due to the largest cell. The process is iterated until no correlation peak can be determined (i.e., correlation coefficient <0.5) in the residual signal.

Figure 6: Decoding result analysis.

(a) Estimated signals are refined based on an optimization algorithm that aims to obtain the best fit between the reconstructed and the original recorded waveform using the least-squares approximation. (b) At the end of the optimization process, the timing and amplitude of calibrated signals accurately reflect the cell parameters measured by high-speed microscopy. (c) Simultaneously recorded high-speed microscopy image validates our results from electrical measurements.

Table 1: Comparison of electrically and optically measured cell parameters of Figure 6b.

To validate our estimations, we optically measured the cell sizes from the high-speed microscopy image. Relative timing between different cells is optically measured from the number of frames between the cells in the high-speed video recorded at 8000 frames per second.

DISCUSSION:

Multiple resistive pulse sensors have previously been incorporated into microfluidic chips²⁸⁻³². In these systems, resistive pulse sensors were either not multiplexed²⁸⁻³¹ or they required individual sensors to be driven at different frequencies³². In both cases, dedicated external connections were needed for each resistive pulse sensor on the chip and therefore a large number of sensors could not be integrated without greater hardware complexity. The important advantage of Microfluidic CODES is that it allows simultaneous reading of multiple resistive pulse sensors from a single output in a simple device. We achieve this by utilizing multiplexing techniques commonly used in telecommunications to design micromachined resistive pulse sensors integrated into microfluidic devices. In essence, our technology relies on code-multiplexing a network of on-chip Coulter counters by designing each to produce a distinguishable signal when a particle is detected. Each micromachined sensor in the network consists of multiple coplanar surface electrodes ordered in differing configurations such that the sequential interaction of flowing particles with these electrodes produces orthogonal impedance modulations waveforms. To accommodate asynchronous particle-sensor interaction, we specifically designed each sensor to produce Gold codes³³, pseudo-orthogonal digital codes that are typically used in the uplink of the CDMA telecommunication networks. Gold codes maintain a certain level orthogonality even when they are misaligned with random phase differences³⁴.

Microfluidic CODES is easily scalable. Although we presented results from a prototype Microfluidic CODES device with four sensors in this paper, more sensors can be incorporated in the device when designed to produce output signals distinguishable from the rest. One way to expand the sensor network is to design sensors based on larger orthogonal code sets with longer digital codes. Longer orthogonal codes with more bits provide higher processing gain in decoding and can be distinguished from each other when there is interference. On the other hand, longer Gold codes in the device also means larger sensing volume, which increases the expected number of interfering sensors. Likewise, increasing the number of sensors for a given sample density will lead to more particles overlapping due to an increase in the overall sensing volume. As such, the density of the particles in the sample is a critical parameter that needs to be considered in using the Microfluidic CODES technology. The maximum particle density that

can be resolved (in analogy with the channel capacity of a CDMA telecommunications network) depends on several factors such as the individual sensor signals and their relation, the decoding scheme, layout of the microfluidic device, and the electronic noise level. Depending on the application, the sample can be diluted to reach a particle density that produces an acceptable error rate.

From signal processing perspective, decoding of time waveforms from a Microfluidic CODES device is not computationally intensive using current systems as evidenced by the fact that cell phone communications on a CDMA network can be demultiplexed in real-time. Furthermore, the physical events to be decoded in microfluidic devices happen much slower than bit transmission rate in cell phone communications allowing us to use more advanced and time-consuming algorithms such as SIC and an optimization processes, which we use to iteratively resolve overlapping signals from sensors.

Taken together, Microfluidic CODES is a versatile, scalable electronic sensing technology that can be readily integrated into various microfluidic devices to realize quantitative assays by tracking particles as they are processed on the chip. The technology is very easy to implement, because (1) it is very simple from a hardware perspective (2) it is directly compatible with the soft lithography (3) it provides a direct electronic read-out without any active on-chip component and (4) it relies on simple computational algorithms for signal processing and data interpretation.

ACKNOWLEDGMENTS:

This work was supported by National Science Foundation Award No. ECCS 1610995. The authors would like to thank the Institute of Electronics and Nanotechnology and the Parker H. Petit Institute for Bioengineering and Bioscience staff for their support in using shared facilities. The authors also would like to thank Chia-Heng Chu for his help in preparing the manuscript.

DISCLOSURES:

The authors have nothing to disclose.

REFERENCES

1. De Roy, K., Clement, L., Thas, O., Wang, Y., & Boon, N. Flow cytometry for fast microbial community fingerprinting. *Water Res.* **46** (3), 907-919, doi:10.1016/j.watres.2011.11.076 (2012).
2. Vives-Rego, J., Lebaron, P., & Nebe-von Caron, G. Current and future applications of flow cytometry in aquatic microbiology. *FEMS Microbiol Rev.* **24** (4), 429-448, doi:10.1111/j.1574-6976.2000.tb00549.x (2000).
3. Alvarez-Barrientos, A., Arroyo, J., Cantón, R., Nombela, C., & Sánchez-Pérez, M. Applications of flow cytometry to clinical microbiology. *Clin Microbiol Rev.* **13** (2), 167-195, doi:10.1128/CMR.13.2.167-195.2000 (2000).
4. Toner, M., & Irimia, D. Blood-on-a-chip. *Annu Rev Biomed Eng.* **7**, 77-103, doi:10.1146/annurev.bioeng.7.011205.135108 (2005).

5. Mehling, M., & Tay, S. Microfluidic cell culture. *Current Opin Biotech.* **25**, 95-102, doi:10.1016/j.copbio.2013.10.005 (2014).
6. Sarioglu, A. F., et al. A microfluidic device for label-free, physical capture of circulating tumor cell clusters. *Nat Methods*, **12** (7), 685-691, doi:10.1038/nmeth.3404 (2015).
7. Cermak N., et al. High-throughput measurement of single-cell growth rates using serial microfluidic mass sensor arrays. *Nat Biotechnol*, doi:10.1038/nbt.3666 (2016).
8. Gossett, D. et al. Label-free cell separation and sorting in microfluidic systems. *Anal Bioanal Chem.* **397** (8), 3249-3267, doi:10.1007/s00216-010-3721-9 (2010).
9. Tsutsui, H. & Ho, C. Cell separation by non-inertial force fields in microfluidic systems. *Mech Res Commun.* **36** (1), 92-103, doi:10.1016/j.mechrescom.2008.08.006 (2009).
10. Edwards, T. L., Gale, B. K., & Frazier, A. B. A microfabricated thermal field-flow fractionation system. *Anal Chem*, **74** (6), 1211-1216, doi:10.1021/ac010653d (2002).
11. Wang, M. M. et al. Microfluidic sorting of mammalian cells by optical force switching. *Nat Biotechnol*, **23** (1), 83-87, doi:10.1038/nbt1050 (2005).
12. Shields IV, C. W., Reyes, C. D., & López, G. P. Microfluidic cell sorting: a review of the advances in the separation of cells from debulking to rare cell isolation. *Lab Chip.* **15** (5), 1230-1249, doi:10.1039/c4lc01246a (2015).
13. Gawad, S., Schild, L., & Renaud, P. Micromachined impedance spectroscopy flow cytometer for cell analysis and particle sizing. *Lab Chip.* **1** (1), 76-82 doi:10.1039/b103933b (2001).
14. Haandbæk, N., Bürgel, S. C., Heer, F., & Hierlemann, A. Characterization of subcellular morphology of single yeast cells using high frequency microfluidic impedance cytometer. *Lab Chip.* **14** (2), 369-377 doi:10.1039/c3lc50866h (2014).
15. Bayley, H. & Martin, C. Resistive-pulse sensing-from microbes to molecules. *Chem Rev.* **100** (7), 2575-2594, doi:10.1021/cr980099g (2000).
16. Polling, D., Deane, S. C., Burcher, M. R., Glasse, C. & Reccius, C. H. Coded electrodes for low signal-noise ratio single cell detection in flow-through impedance spectroscopy. *Proceedings of uTAS* (The 14th International Conference on Miniaturized Systems for Chemistry and Life Sciences), October 3-7, 2010, Groningen, The Netherlands.
17. Javanmard, M., & Davis, R. W. Coded corrugated microfluidic sidewalls for code division multiplexing. *IEEE Sensors J.* **13** (5), 1399-1400, doi:10.1109/JSEN.2013.2242396 (2013).
18. Balakrishnan, K. R. et al. Node-pore sensing: a robust, high-dynamic range method for detecting biological species. *Lab Chip.* **13** (7), 1302-1307, doi:10.1039/c3lc41286e (2013).
19. Emaminejad, S., Talebi, S., Davis, R. W., & Javanmard, M. Multielectrode sensing for extraction of signal from noise in impedance cytometry. *IEEE Sensors J.* **15** (5), 2715-2716 doi:10.1109/JSEN.2015.2389224 (2015).
20. Spencer, D., Caselli, F., Bisegna, P., & Morgan, H. (2016). High accuracy particle analysis using sheathless microfluidic impedance cytometry. *Lab Chip.* **16**, 2467-2473, doi:10.1039/c6lc00339g (2016).
21. Liu, R., Wang, N., Kamili, F. & Sarioglu, A. Microfluidic CODES: a scalable multiplexed electronic sensor for orthogonal detection of particles in microfluidic channels. *Lab Chip.* **16** (8), 1350-1357, doi:10.1039/c6lc00209a (2016).
22. Buehrer, R. Code Division Multiple Access(CDMA). *Synthesis Lectures on Communications.* **1** (1), 1-192, doi:10.2200/s00017ed1v01y200508com002 (2006).
23. Proakis, J. *Digital Communications*, McGraw-Hill, New York, NY (1989).

24. Patel, P. & Holtzman, J. Analysis of a simple successive interference cancellation scheme in a DS/CDMA system. *IEEE J Sel Areas Commun.* **12** (5), 796-807 (1994).
25. Hui, A. & Letaief, K. Successive interference cancellation for multiuser asynchronous DS/CDMA detectors in multipath fading links. *IEEE Trans Commun.* **46** (3), 384-391, doi:10.1109/26.662644 (1998).
26. Prediction and regulation by linear least-square methods. *J Macroecon.* **7** (1), 126 (1985).
27. Whitesides, G., Ostuni, E., Takayama, S., Jiang, X. & Ingber, D. Soft lithography in biology and biochemistry. *Annu Rev Biomed Eng.* **3** (1), 335-373, doi:10.1146/annurev.bioeng.3.1.335 (2001).
28. Zhe, J., Jagtiani, A., Dutta, P., Hu, J. & Carletta, J. A micromachined high throughput Coulter counter for bioparticle detection and counting. *J Micromech Microeng.* **17** (2), 304-313, doi:10.1088/0960-1317/17/2/017 (2007).
29. Song, Y., Yang, J., Pan, X. & Li, D. High-throughput and sensitive particle counting by a novel microfluidic differential resistive pulse sensor with multidetecting channels and a common reference channel. *Electrophoresis.* **36** (4), 495-501 (2015).
30. Watkins, N. et al. Microfluidic CD4+ and CD8+ T lymphocyte counters for point-of-care HIV diagnostics using whole blood. *Sci Transl Med.* **5** (214), 214ra170-214ra170 (2013).
31. Chen, Y. et al. Portable Coulter counter with vertical through-holes for high-throughput applications. *Sensor Actuat B-Chem*, **213**, 375-381 (2015).
32. Jagtiani, A., Carletta, J. & Zhe, J. An impedimetric approach for accurate particle sizing using a microfluidic Coulter counter. *J Micromech Microeng.* **21** (4), 045036 (2011).
33. Gold, R. Optimal binary sequences for spread spectrum multiplexing (Corresp.). *IEEE Trans. Inform. Theory.* **13** (4), 619-621 (1967).
34. Dinan, E. & Jabbari, B. Spreading codes for direct sequence CDMA and wideband CDMA cellular networks. *IEEE Commun Mag.* **36** (9), 48-54 (1998).

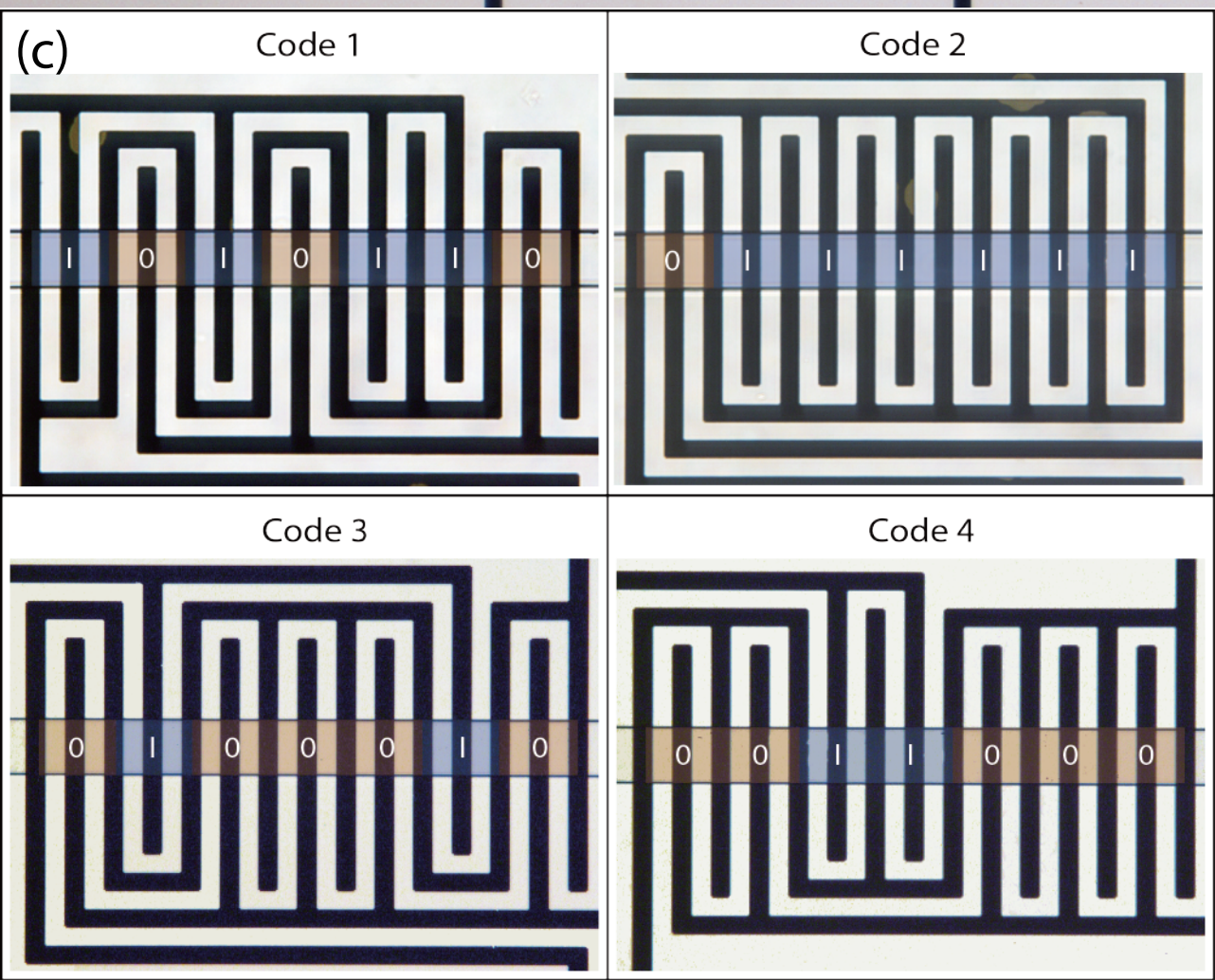
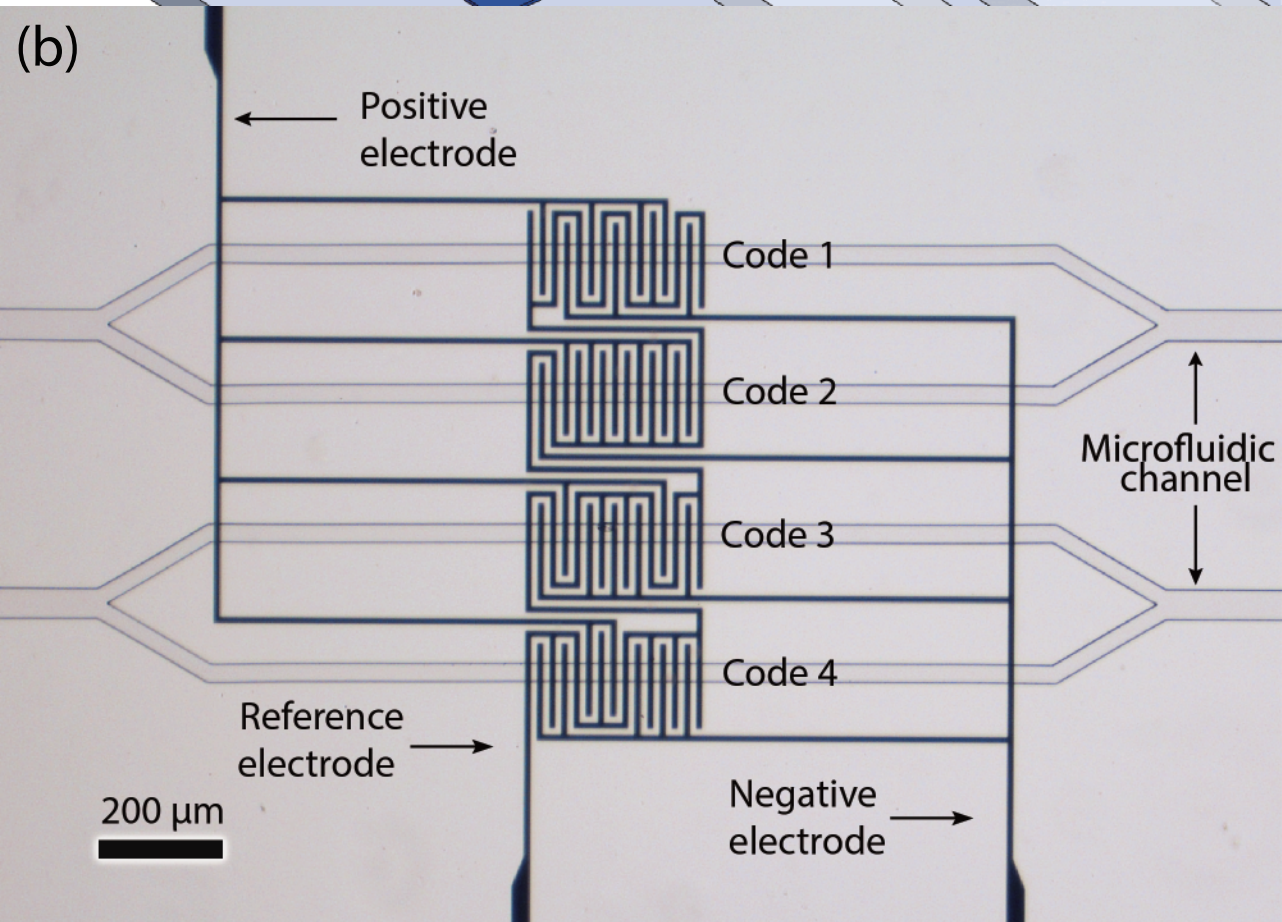
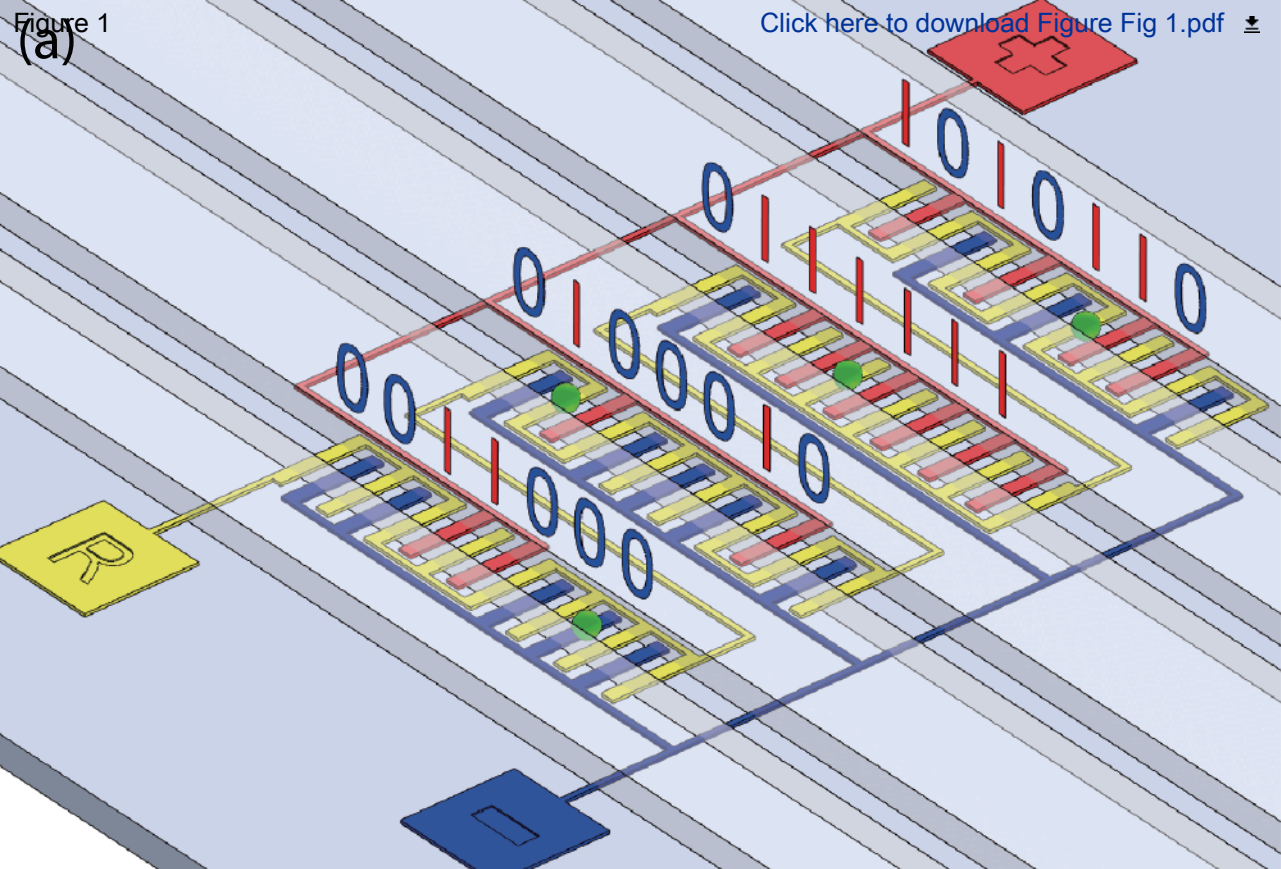


Figure 2

[Click here to download Figure Fig 2.pdf](#)

(a)

1- Spin photoresist on silicon



2- Photolithography



3- Spin and cure PDMS



4- Demold

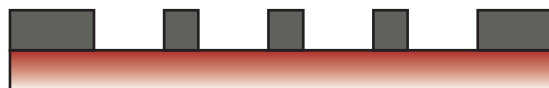


(b)

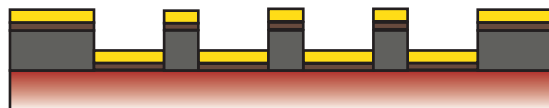
1- Spin photoresist on glass



2- Photolithography



3- E-beam deposition

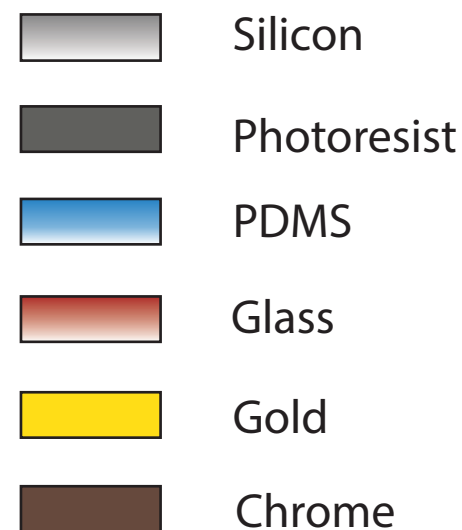


4- Lift-off



(c)

Final device assembly



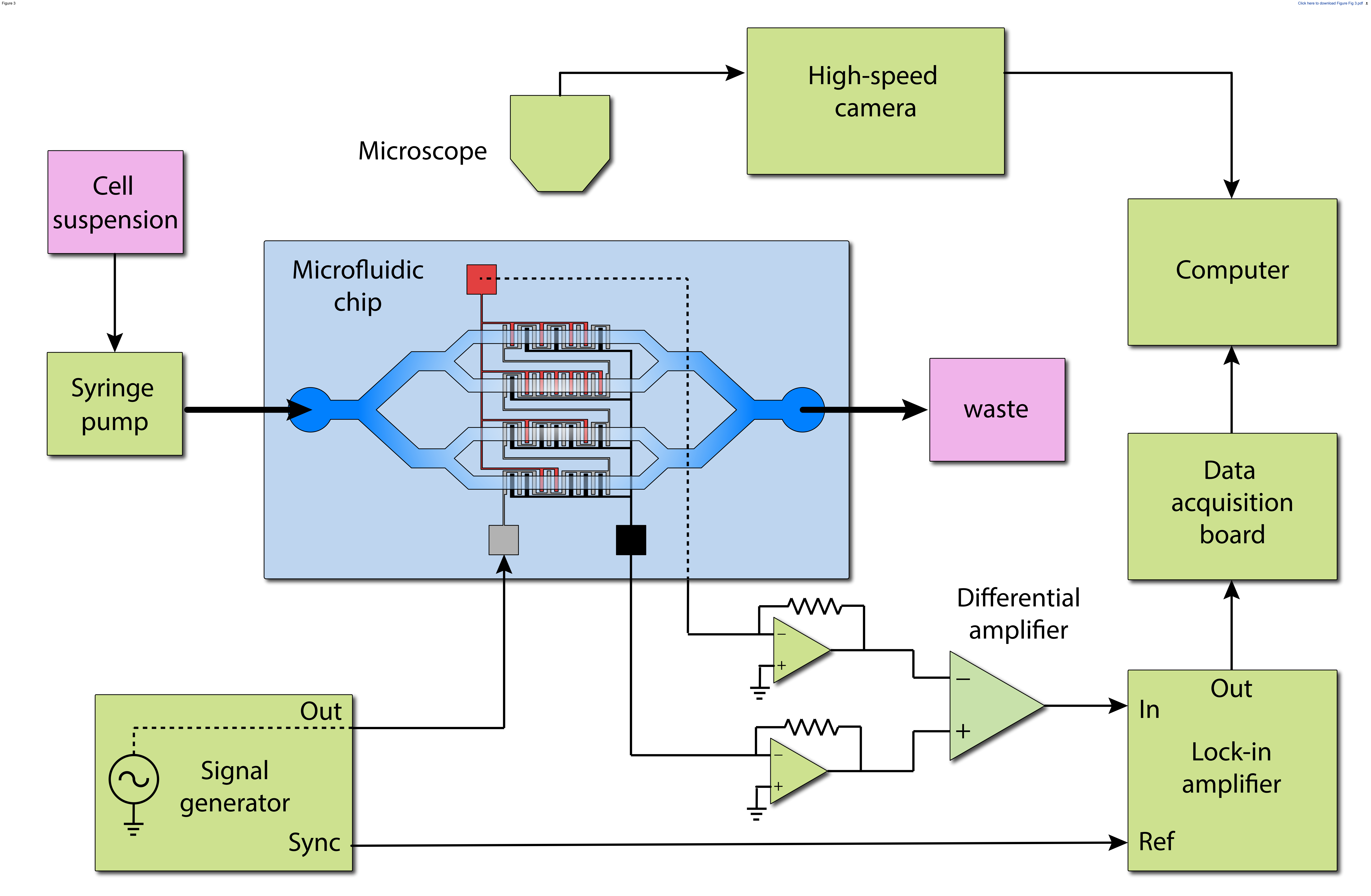
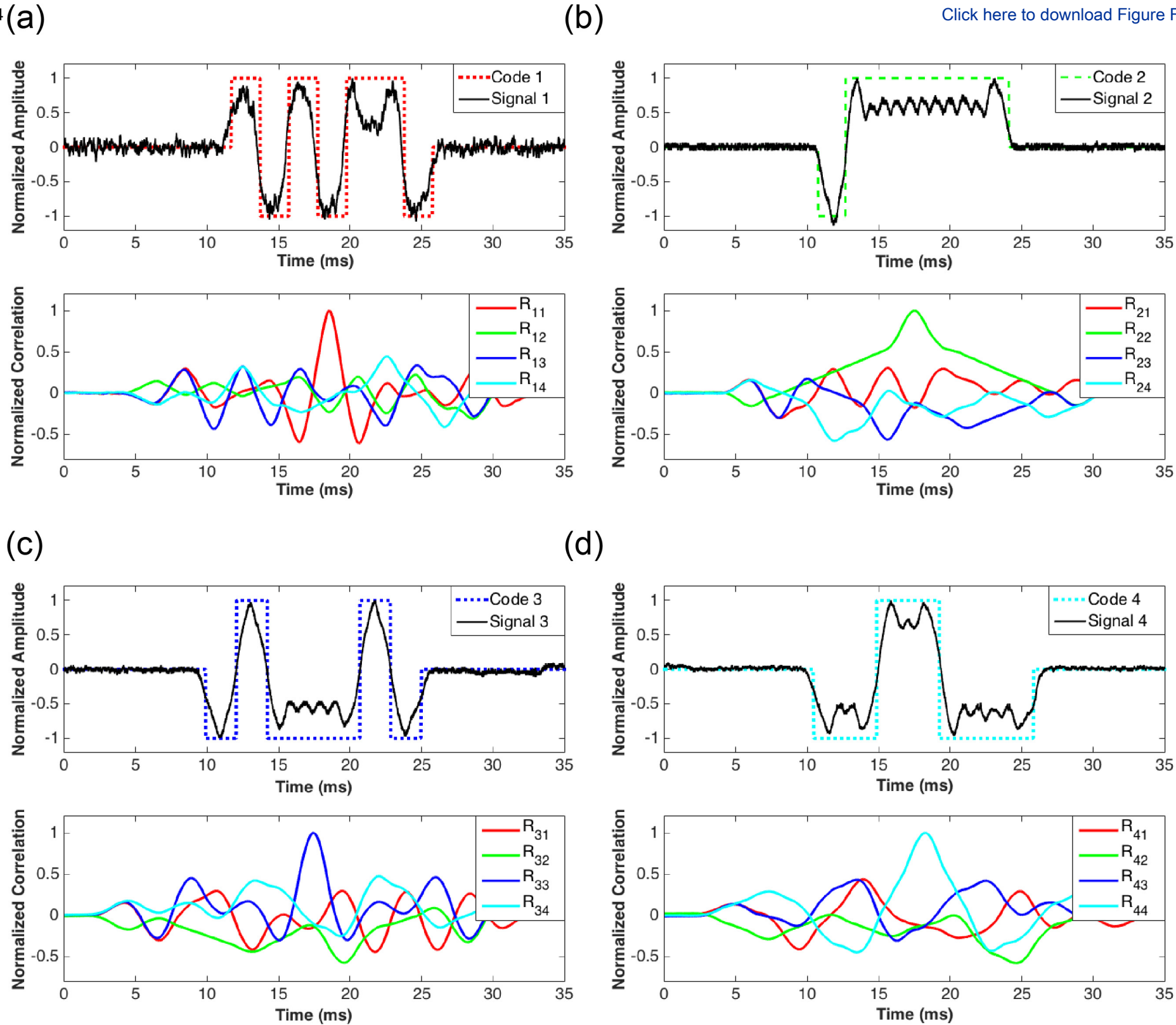
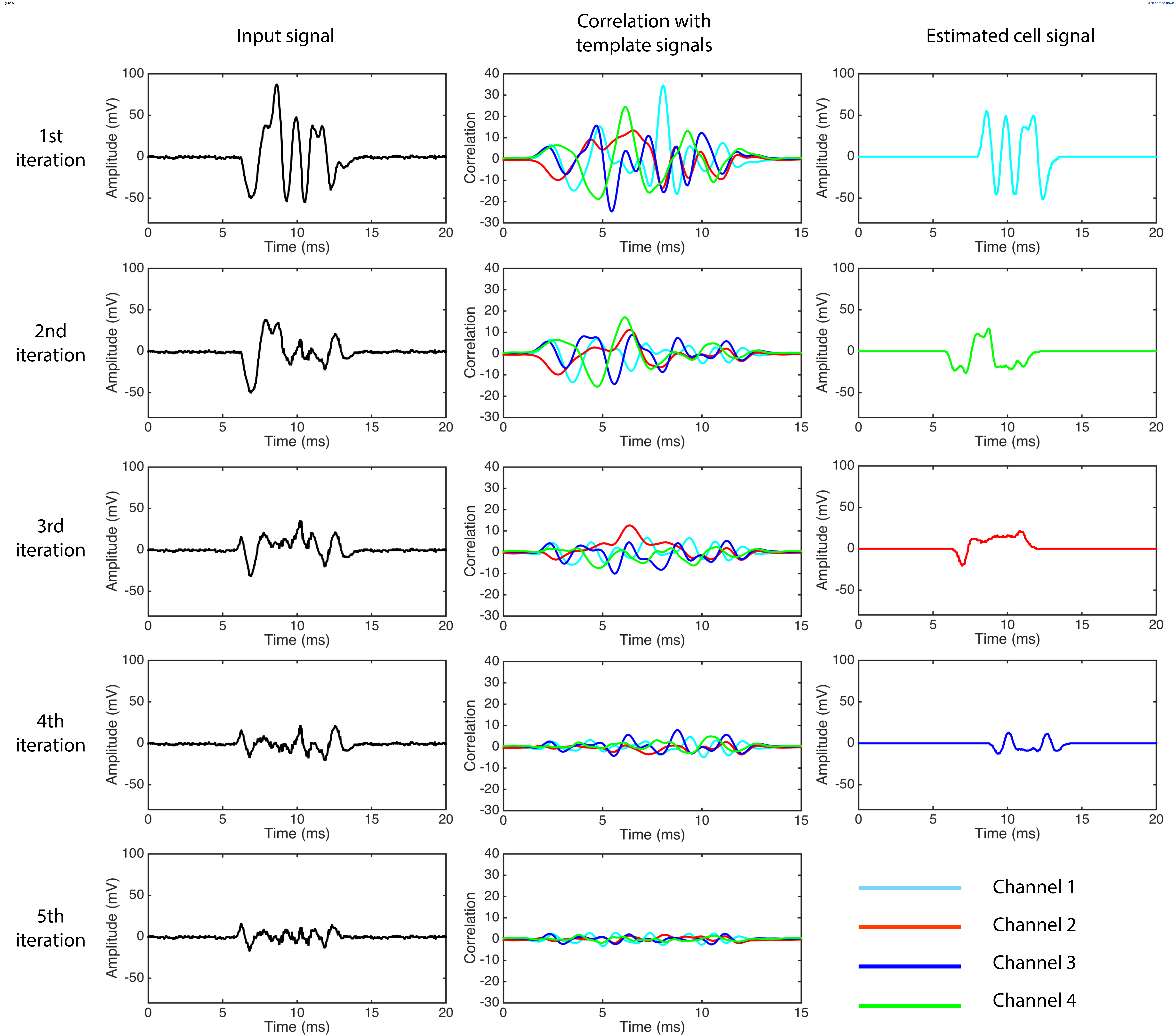
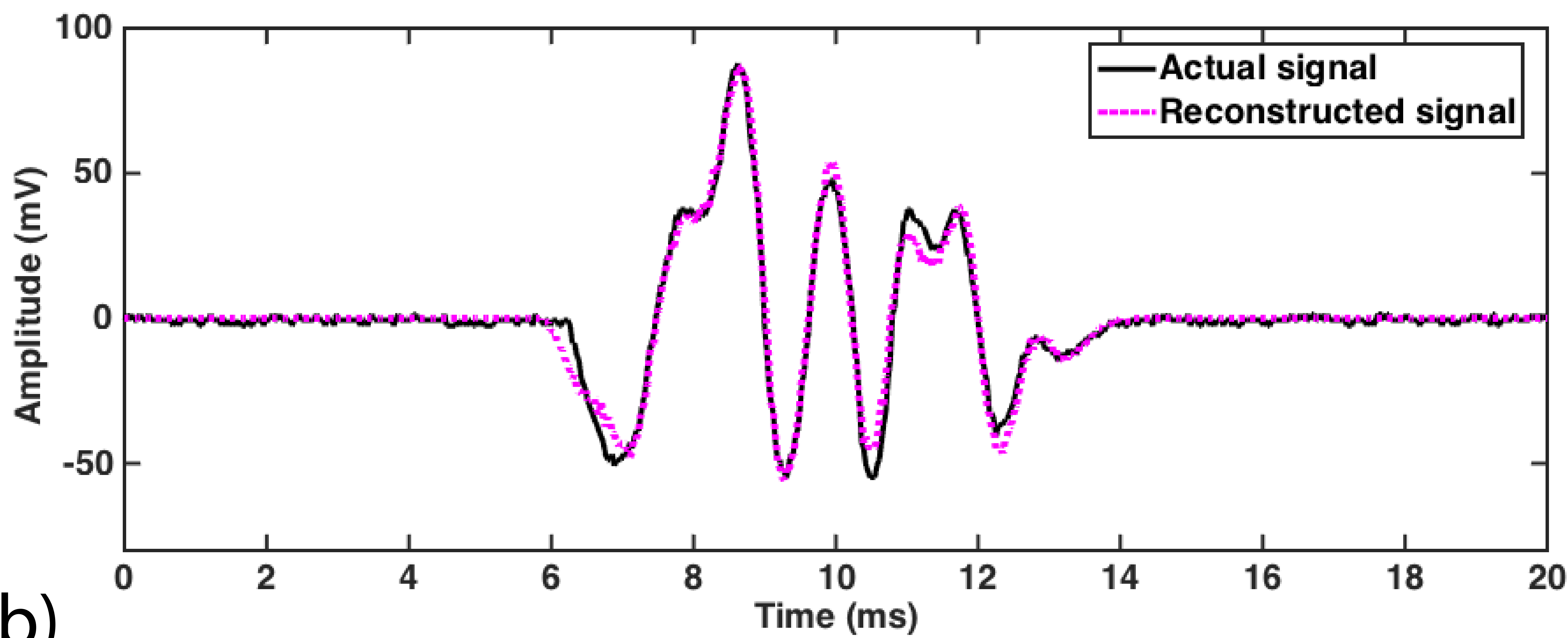


Figure 4

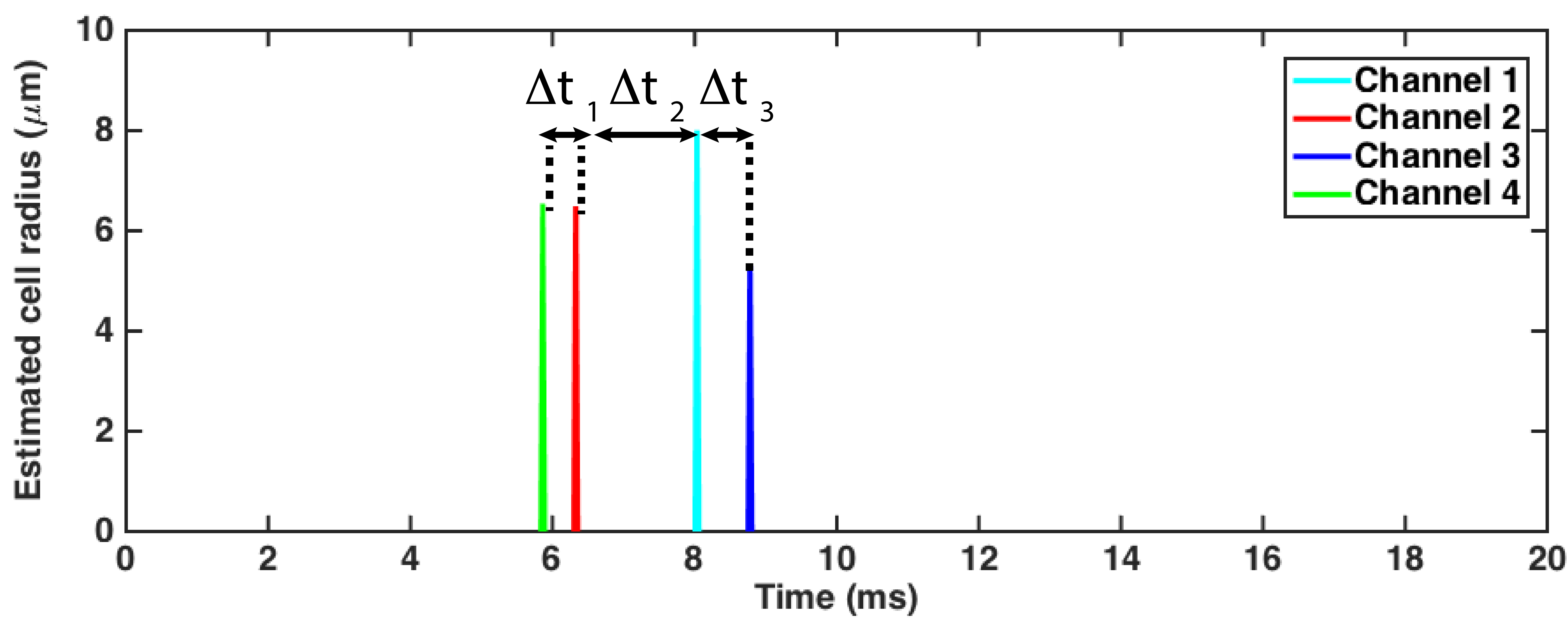




(a)



(b)



(c)

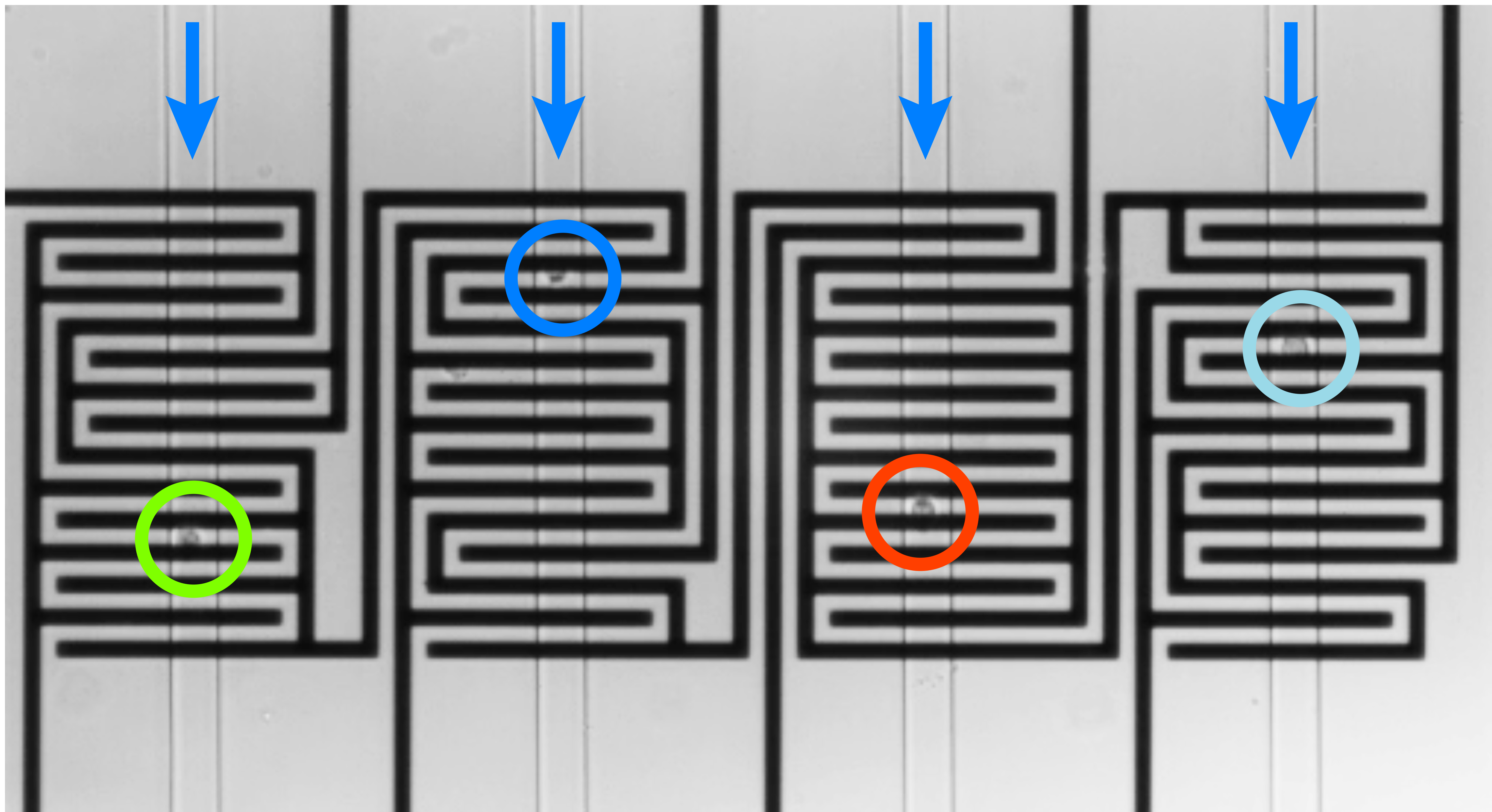


Table 1

Measurement type	$r_{ch1} (\mu m)$	$r_{ch2} (\mu m)$	$r_{ch3} (\mu m)$	$r_{ch4} (\mu m)$	$\Delta t_1 (ms)$	$\Delta t_2 (ms)$	$\Delta t_3 (ms)$
Electrical	8.010	6.490	5.300	6.550	0.465	1.705	0.744
Optical	8.320	6.770	5.680	7.040	0.375	1.625	0.750

Name of Material/ Equipment	Company	Catalog Number	Comments/Description
98% Sulfuric Acid	BDH Chemicals	BDH3074-3.8LP	Sylgard 184 Silicone Elastomer Kit
30% Hydrogen Peroxide	BDH Chemicals	BDH7690-3	
Trichlorosilane	Aldrich Chemistry	235725-100G	
NR9-1500PY Negative Photoresist	Furuttex		
Resist Developer RD6	Furuttex		
Acetone	BDH Chemicals	BDH1101-4LP	
SU-8 2015 Negative Photoresist	Microchem	SU8-2015	
SU-8 Developer	Microchem	Y010200	
Polydimethylsiloxane (PDMS)	Dow Corning	3097358-1004	
Isopropyl Alcohol	BDH Chemicals	BDH1133-4LP	
RPMI 1640	Corning Cellgro	10-040-CV	
Fetal Bovine Serum (FBS)	Seradigm	1500-050	
Penicillin-Streptomycin	Amresco	K952-100ML	
Phosphate-Buffered Saline (PBS)	Corning Cellgro	21-040-CM	
PHD 22/2000 Syringe Pump	Harvard Apparatus	70-2001	
HF2LI Lock-in Amplifier	Zurich Instrument		
HF2TA Current Amplifier	Zurich Instrument		
Eclipse Ti-U Microscope	Nikon Corporation		
DS-Fi2 High-Definition Color Camera	Nikon Corporation		
v7.3 High-speed Camera	Phantom		
PCle-6361 Data Acquisition Board	National Instruments	781050-01	
BNC-2120 Shielded Connector Block	National Instruments	777960-01	
PX-250 Plasma Treatment System	Nordson MARCH		



1 Alewife Center #200
Cambridge, MA 02140
tel. 617.945.9051
www.jove.com

ARTICLE AND VIDEO LICENSE AGREEMENT

Title of Article:

Author(s):

Item 1 (check one box): The Author elects to have the Materials be made available (as described at <http://www.jove.com/publish>) via: ☒ Standard Access ☐ Open Access

Item 2 (check one box):

- ☒ The Author is NOT a United States government employee.
- ☐ The Author is a United States government employee and the Materials were prepared in the course of his or her duties as a United States government employee.
- ☐ The Author is a United States government employee but the Materials were NOT prepared in the course of his or her duties as a United States government employee.

ARTICLE AND VIDEO LICENSE AGREEMENT

1. Defined Terms. As used in this Article and Video License Agreement, the following terms shall have the following meanings: “**Agreement**” means this Article and Video License Agreement; “**Article**” means the article specified on the last page of this Agreement, including any associated materials such as texts, figures, tables, artwork, abstracts, or summaries contained therein; “**Author**” means the author who is a signatory to this Agreement; “**Collective Work**” means a work, such as a periodical issue, anthology or encyclopedia, in which the Materials in their entirety in unmodified form, along with a number of other contributions, constituting separate and independent works in themselves, are assembled into a collective whole; “**CRC License**” means the Creative Commons Attribution-Non Commercial-No Derivs 3.0 Unported Agreement, the terms and conditions of which can be found at: <http://creativecommons.org/licenses/by-nc-nd/3.0/legalcode>; “**Derivative Work**” means a work based upon the Materials or upon the Materials and other pre-existing works, such as a translation, musical arrangement, dramatization, fictionalization, motion picture version, sound recording, art reproduction, abridgment, condensation, or any other form in which the Materials may be recast, transformed, or adapted; “**Institution**” means the institution, listed on the last page of this Agreement, by which the Author was employed at the time of the creation of the Materials; “**JoVE**” means MyJoVE Corporation, a Massachusetts corporation and the publisher of *The Journal of Visualized Experiments*; “**Materials**” means the Article and / or the Video; “**Parties**” means the Author and JoVE; “**Video**” means any video(s) made by the Author, alone or in conjunction with any other parties, or by JoVE or its affiliates or agents, individually or in collaboration with the Author or any other parties, incorporating all or any portion of the Article, and in which the Author may or may not appear.

2. Background. The Author, who is the author of the Article, in order to ensure the dissemination and protection of the Article, desires to have the JoVE publish the Article and create and transmit videos based on the Article. In furtherance of such goals, the Parties desire to memorialize in this Agreement the respective rights of each Party in and to the Article and the Video.

3. Grant of Rights in Article. In consideration of JoVE agreeing to publish the Article, the Author hereby grants to JoVE, subject to **Sections 4 and 7** below, the exclusive, royalty-free, perpetual (for the full term of copyright in the Article, including any extensions thereto) license (a) to publish, reproduce, distribute, display and store the Article in all forms, formats and media whether now known or hereafter developed (including without limitation in print, digital and electronic form) throughout the world, (b) to translate the Article into other languages, create adaptations, summaries or extracts of the Article or other Derivative Works (including, without limitation, the Video) or Collective Works based on all or any portion of the Article and exercise all of the rights set forth in (a) above in such translations, adaptations, summaries, extracts, Derivative Works or Collective Works and (c) to license others to do any or all of the above. The foregoing rights may be exercised in all media and formats, whether now known or hereafter devised, and include the right to make such modifications as are technically necessary to exercise the rights in other media and formats. If the “Open Access” box has been checked in **Item 1** above, JoVE and the Author hereby grant to the public all such rights in the Article as provided in, but subject to all limitations and requirements set forth in, the CRC License.

ARTICLE AND VIDEO LICENSE AGREEMENT

4. Retention of Rights in Article. Notwithstanding the exclusive license granted to JoVE in **Section 3** above, the Author shall, with respect to the Article, retain the non-exclusive right to use all or part of the Article for the non-commercial purpose of giving lectures, presentations or teaching classes, and to post a copy of the Article on the Institution's website or the Author's personal website, in each case provided that a link to the Article on the JoVE website is provided and notice of JoVE's copyright in the Article is included. All non-copyright intellectual property rights in and to the Article, such as patent rights, shall remain with the Author.

5. Grant of Rights in Video – Standard Access. This **Section 5** applies if the "Standard Access" box has been checked in **Item 1** above or if no box has been checked in **Item 1** above. In consideration of JoVE agreeing to produce, display or otherwise assist with the Video, the Author hereby acknowledges and agrees that, Subject to **Section 7** below, JoVE is and shall be the sole and exclusive owner of all rights of any nature, including, without limitation, all copyrights, in and to the Video. To the extent that, by law, the Author is deemed, now or at any time in the future, to have any rights of any nature in or to the Video, the Author hereby disclaims all such rights and transfers all such rights to JoVE.

6. Grant of Rights in Video – Open Access. This **Section 6** applies only if the "Open Access" box has been checked in **Item 1** above. In consideration of JoVE agreeing to produce, display or otherwise assist with the Video, the Author hereby grants to JoVE, subject to **Section 7** below, the exclusive, royalty-free, perpetual (for the full term of copyright in the Article, including any extensions thereto) license (a) to publish, reproduce, distribute, display and store the Video in all forms, formats and media whether now known or hereafter developed (including without limitation in print, digital and electronic form) throughout the world, (b) to translate the Video into other languages, create adaptations, summaries or extracts of the Video or other Derivative Works or Collective Works based on all or any portion of the Video and exercise all of the rights set forth in (a) above in such translations, adaptations, summaries, extracts, Derivative Works or Collective Works and (c) to license others to do any or all of the above. The foregoing rights may be exercised in all media and formats, whether now known or hereafter devised, and include the right to make such modifications as are technically necessary to exercise the rights in other media and formats. For any Video to which this Section 6 is applicable, JoVE and the Author hereby grant to the public all such rights in the Video as provided in, but subject to all limitations and requirements set forth in, the CRC License.

7. Government Employees. If the Author is a United States government employee and the Article was prepared in the course of his or her duties as a United States government employee, as indicated in **Item 2** above, and any of the licenses or grants granted by the Author hereunder exceed the scope of the 17 U.S.C. 403, then the rights granted hereunder shall be limited to the maximum rights permitted under such

statute. In such case, all provisions contained herein that are not in conflict with such statute shall remain in full force and effect, and all provisions contained herein that do so conflict shall be deemed to be amended so as to provide to JoVE the maximum rights permissible within such statute.

8. Likeness, Privacy, Personality. The Author hereby grants JoVE the right to use the Author's name, voice, likeness, picture, photograph, image, biography and performance in any way, commercial or otherwise, in connection with the Materials and the sale, promotion and distribution thereof. The Author hereby waives any and all rights he or she may have, relating to his or her appearance in the Video or otherwise relating to the Materials, under all applicable privacy, likeness, personality or similar laws.

9. Author Warranties. The Author represents and warrants that the Article is original, that it has not been published, that the copyright interest is owned by the Author (or, if more than one author is listed at the beginning of this Agreement, by such authors collectively) and has not been assigned, licensed, or otherwise transferred to any other party. The Author represents and warrants that the author(s) listed at the top of this Agreement are the only authors of the Materials. If more than one author is listed at the top of this Agreement and if any such author has not entered into a separate Article and Video License Agreement with JoVE relating to the Materials, the Author represents and warrants that the Author has been authorized by each of the other such authors to execute this Agreement on his or her behalf and to bind him or her with respect to the terms of this Agreement as if each of them had been a party hereto as an Author. The Author warrants that the use, reproduction, distribution, public or private performance or display, and/or modification of all or any portion of the Materials does not and will not violate, infringe and/or misappropriate the patent, trademark, intellectual property or other rights of any third party. The Author represents and warrants that it has and will continue to comply with all government, institutional and other regulations, including, without limitation all institutional, laboratory, hospital, ethical, human and animal treatment, privacy, and all other rules, regulations, laws, procedures or guidelines, applicable to the Materials, and that all research involving human and animal subjects has been approved by the Author's relevant institutional review board.

10. JoVE Discretion. If the Author requests the assistance of JoVE in producing the Video in the Author's facility, the Author shall ensure that the presence of JoVE employees, agents or independent contractors is in accordance with the relevant regulations of the Author's institution. If more than one author is listed at the beginning of this Agreement, JoVE may, in its sole discretion, elect not take any action with respect to the Article until such time as it has received complete, executed Article and Video License Agreements from each such author. JoVE reserves the right, in its absolute and sole discretion and without giving any reason therefore, to accept or decline any work submitted to JoVE. JoVE and its employees, agents and independent contractors shall have

ARTICLE AND VIDEO LICENSE AGREEMENT

full, unfettered access to the facilities of the Author or of the Author's institution as necessary to make the Video, whether actually published or not. JoVE has sole discretion as to the method of making and publishing the Materials, including, without limitation, to all decisions regarding editing, lighting, filming, timing of publication, if any, length, quality, content and the like.

11. **Indemnification.** The Author agrees to indemnify JoVE and/or its successors and assigns from and against any and all claims, costs, and expenses, including attorney's fees, arising out of any breach of any warranty or other representations contained herein. The Author further agrees to indemnify and hold harmless JoVE from and against any and all claims, costs, and expenses, including attorney's fees, resulting from the breach by the Author of any representation or warranty contained herein or from allegations or instances of violation of intellectual property rights, damage to the Author's or the Author's institution's facilities, fraud, libel, defamation, research, equipment, experiments, property damage, personal injury, violations of institutional, laboratory, hospital, ethical, human and animal treatment, privacy or other rules, regulations, laws, procedures or guidelines, liabilities and other losses or damages related in any way to the submission of work to JoVE, making of videos by JoVE, or publication in JoVE or elsewhere by JoVE. The Author shall be responsible for, and shall hold JoVE harmless from, damages caused by lack of sterilization, lack of cleanliness or by contamination due to the making of a video by JoVE its employees, agents or independent contractors. All sterilization, cleanliness or decontamination procedures shall be solely the responsibility of the Author and shall be undertaken at the Author's


expense. All indemnifications provided herein shall include JoVE's attorney's fees and costs related to said losses or damages. Such indemnification and holding harmless shall include such losses or damages incurred by, or in connection with, acts or omissions of JoVE, its employees, agents or independent contractors.

12. **Fees.** To cover the cost incurred for publication, JoVE must receive payment before production and publication the Materials. Payment is due in 21 days of invoice. Should the Materials not be published due to an editorial or production decision, these funds will be returned to the Author. Withdrawal by the Author of any submitted Materials after final peer review approval will result in a US\$1,200 fee to cover pre-production expenses incurred by JoVE. If payment is not received by the completion of filming, production and publication of the Materials will be suspended until payment is received.

13. **Transfer, Governing Law.** This Agreement may be assigned by JoVE and shall inure to the benefits of any of JoVE's successors and assignees. This Agreement shall be governed and construed by the internal laws of the Commonwealth of Massachusetts without giving effect to any conflict of law provision thereunder. This Agreement may be executed in counterparts, each of which shall be deemed an original, but all of which together shall be deemed to be one and the same agreement. A signed copy of this Agreement delivered by facsimile, e-mail or other means of electronic transmission shall be deemed to have the same legal effect as delivery of an original signed copy of this Agreement.

A signed copy of this document must be sent with all new submissions. Only one Agreement required per submission.

CORRESPONDING AUTHOR:

Name:	Ali Fatih Sarioglu	
Department:	School of Electrical and Computer Engineering	
Institution:	Georgia Institute of Technology	
Article Title:	Microfluidic platform with multiplexed electronic detection for spatial tracking of particles	
Signature:		Date: 7/25/2016

Please submit a signed and dated copy of this license by one of the following three methods:

- 1) Upload a scanned copy of the document as a pdf on the JoVE submission site;
- 2) Fax the document to +1.866.381.2236;
- 3) Mail the document to JoVE / Attn: JoVE Editorial / 1 Alewife Center #200 / Cambridge, MA 02139

For questions, please email submissions@jove.com or call +1.617.945.9051

Editor:

Questions/Concerns:

1 - Please take this opportunity to thoroughly proofread the manuscript to ensure that there are no spelling or grammar issues. The JoVE editor will not copy-edit your manuscript and any errors in the submitted revision may be present in the published version.

We have proofread the manuscript and we are sure that there are no spelling or grammar issues.

2. Please abbreviate all journal titles.

We have abbreviated all the journal titles.

3. Length is at maximum limit.

We added concise information to the manuscript while making suggested revisions.

4. Grammar: Line 51 – “the Microfluidic CODES”

We have modified this sentence. (See lines 51-52).

5. Additional detail is required:

-Section 1 – Please provide a citation as insufficient detail is supplied to replicate the design.

We have added a citation about designing Gold codes in the first step of section 1. (See line 106).

-2.7 – What settings are used for deposition?

We used an automated e-beam evaporator (Denton Explorer) for metal deposition in our work. Denton Explorer was given deposition rate and target metal thickness as only inputs. We have added the deposition rate and base pressure recorded during deposition to the manuscript in lines 153-155.

-2.8 – What constitutes “mild sonication”?

We used a conventional normal ultrasonic bath machine for sonication, with non-controllable power setting. In lines 157-159, we have revised the sentence into “...sonication with frequency 40 kHz at 100% amplitude for 30 min at room temperature...” to describe the sonication process conditions.

-3.10 – How is this done?

We dispense 200 μL of trichlorosilane in a petri dish and placed it in a vacuum desiccator together with the SU-8 mold at room temperature. The SU-8 mold was kept under vacuum (94.8 kPa) for 8 hours to facilitate coating of the mold surface with trichlorosilane molecules in vapor-phase. (See lines 203-205).

-4.3 – Approximately what size should the pieces be?

The sizes of the cut PDMS pieces are approximately 20 mm \times 7 mm. We revised the text to provide this information. (See lines 215-218).

-4.7 – How is bonding performed?

Plasma-activated glass substrate and PDMS bonds spontaneously when brought in physical contact. We revised the text to clarify this point. (See lines 228-229).

-6.3 – What flow rate is used?

In our experiments, we used flow rates ranging from 50 $\mu\text{L}/\text{h}$ to 1000 $\mu\text{L}/\text{h}$. We revised the text to provide this information. (See lines 274-275).

-Section 6 – Please indicate how different pieces are connected to the chip. Should these connections be performed prior to flowing cells into the chip? If so, Step 6.3 should appear much later in the section.

Yes, electrical connections to the chip should be performed prior to flowing cells into the chip. We revised the order of procedures to clarify this point. (See lines 262-275).

-Section 7 – How are these things done in the software? Please provide the code as a supplemental file or include a citation containing instructions on how to do these analyses in the software.

We have added a more detailed description about the signal processing part and explicitly stated built-in MATLAB functions used in our mathematical calculations. We also included references for specific decoding or optimization algorithms mentioned in the protocol. (See lines 296-338).

6. Results: Figure 4 legend – Please describe what is shown in each panel. What are the differences among them?

We revised the figure caption to describe plots in each panel. (See lines 422-430).

7. Discussion: Please discuss the significance with respect to alternative methods. Please also discuss the limitations of the method.

We revised the manuscript to discuss the significance of our technology with respect to alternative methods in the first paragraph of the discussion. (See lines 457-463).

Reviewer #1:

Questions/Concerns:

I recommend that in the introduction that the authors make sure to highlight and mention previous works from different groups which have also made use of multiple electrodes and corrugated channels prior to CODES to make the readers familiar with the field and to know how the idea of using multiple electrodes for improvements in performance has evolved over the last 5-7 years. This will also be useful so that the readers will know the different applications of these various multi-electrode schemes. Here are references I recommend the authors include:

1. Spencer D, Caselli F, Bisegna P, Morgan H. High accuracy particle analysis using sheathless microfluidic impedance cytometry. Lab on a Chip. 2016.
2. D. Polling, S. C. Deane, M. R. Burcher, C. Glasse and C. H. Reccius, Proceedings of uTAS (The 14th International Conference on Miniaturized Systems for Chemistry and Life Sciences), October 3-7, 2010, Groningen, The Netherlands
3. M. Javanmard and R. W. Davis, IEEE Sens. J., 2013, 13, 1399-1400.
4. K. R. Balakrishnan, G. Anwar, M. R. Chapman, T. Nguyen, A. Kesavaraju and L. L. Sohn, Lab Chip, 2013, 13, 1302-1307 .
5. S. Emaminejad, S. Talebi, R. W. Davis and M. Javanmard, IEEE Sens. J., 2015, 15, 2715-2716
6. P. Kiesel, M. Bassler, M. Beck and N. Johnson, Appl. Phys. Lett., 2009, 94, 041107
7. J. Martini, M. I. Recht, M. Huck, M. W. Bern, N. M. Johnson and P. Kiesel, Lab Chip, 2012, 12, 5057-5062 .

Also, I think it would be good to include 5-10 more references on more contemporary applications of impedance cytometry for proteomics, smart electroporation, nucleic acid analysis, virus detection, etc... so that readers will appreciate the broader impacts that CODES can have.

Aside from these minor points, this is excellent work.

We revised to text to add additional references as suggested by the Reviewer.

Reviewer #2:

Questions/Concerns:

1 - What is the scalability of the SIC process when more and more channels are added for large-scale cell sorting architectures? Because the correlation of each channel must be done in succession, i.e. serially, it is not a parallel process and for large number of channels the time to process signals from all channels will add up. How does this limit the overall sorting speed per number of channels? Or is signal processing not a limitation due to fast computing speeds available?

We thank the Referee for pointing to the need to explain this point. Signal processing speed is not a limitation in our system. We revised the text to discuss this issue. (See lines 493-499).

2. Can the fluidic channels be fabricated to control the cell flow so they are in each channel one by one? E.g. size dependent cell sorter. If not, in the event of 2 similar cells passing parallel to each other in a channel, are they distinguishable or would they show up as a strong correlation signal, hence a big cell? This seems like a problem as this is mentioned in lines 453-461 in discussion.

We thank the Referee for pointing to the need to clarify this important point. In our device, the cross section of the microfluidic channels is designed to be close to the cell size so that two cells cannot simultaneously pass over a sensor in parallel. We revised the text to clarify this point. (See lines 342-345).

3. How orthogonal do the codes have to be before signal differentiation by correlation peak detection becomes poor? Ex. For 1010110 and 1010111, how distinguishable will they be in this system? I would imagine when scaling to more channels, highly orthogonal codes (such as 1010110 and 0111111 as used here) would be ideal as mentioned in lines 446-451. When the codes are increased in length to keep them highly orthogonal, does this have negative consequences? What is a practical limit on this code length to make the system speedy yet easy to signal process?

Orthogonal codes are easier to distinguish due to minimal cross-correlation. However, the codes should also be chosen such that they remain orthogonal under random phase shifts when sensors asynchronously interfere. Gold codes have this feature. We revised the text to clarify this point. (See lines 472-474). The Reviewer is right, to obtain more orthogonal codes to multiplex more channels, we need longer codes. However, longer codes lead to higher sensing volume and increase the likelihood of interference for a given sample density. We revised the to explain this trade-off. (See lines 478-486). The longer codes will not affect the signal processing speed directly.

4. Figure 6 legend should be corrected: singal -> signal

We thank the Referee for pointing out this error. We now revised the legend of Figure 6.

5. What is the main difference between this paper and work presented in Lab Chip?

Lab Chip paper was the first introduction of the Microfluidic CODES technology. In that paper, we mainly focused on the principle of operation of the sensor, and presented our experimental results. In this paper, our goal is to make this technology available to our researchers so that they can use it for their applications. Therefore, we present a detailed protocol that explains individual steps in design of devices, microfabrication process, culturing of cell lines, constructing the experimental setup and signal processing. Some of the figures in the paper were adapted from the Lab Chip paper as supportive materials for explaining the protocol. Moreover, due to its video paper format, Journal of Visualized Experiments provides the optimum channel to fully demonstrate the capabilities of our method. We revised the manuscript to explicitly state this point. (See lines 93-100).